Evolution of electronic bandgap by anion variation to explore niobium new halide double perovskites Cs_2GeNbX_6 (X = Cl, Br, I) for solar cells and thermoelectric applications: first principles analysis

A. Labdelli[a,b,*], F. Bendahma[c], M. Mana[d] and N. Benderdouche[e]

[a]*Biotechnology Applied to Agriculture and Environment Preservation Laboratory (L.B.A.A.P.E).*
[b]*Higher School of Agronomy, Mostaganem, Algeria.*
[c]*Laboratory of Technology and Solid Properties, Abdelhamid Ibn Badis University, 27000 Mostaganem, Algeria.*
[d]*Abdelhamid Ibn Badis University, 27000 Mostaganem, Algeria.*
[e]*Laboratory of Structure, Development and Application of Molecular Materials (SEA2M), Abdelhamid Ibn Badis University, 27000 Mostaganem, Algeria.*

Received 4 March 2023; accepted 17 May 2023

The structural, electronic, optical, and thermoelectric properties of the niobium new halide double perovskites Cs_2GeNbX_6 (X = Cl, Br, I) were investigated using a density functional theory method. The generalized gradient approximation (GGA-PBE) method is used to project the exchange-correlation potential. The tolerance factor and optimizing total energy define the structure's stability. The magnetic moments of our compounds are high, more than 3 μ_B. The compounds have direct narrow band gaps of 0.69, 0.46, and 0.26 eV, respectively, for $Cs_2GeNbCl_6$, $Cs_2GeNbBr_6$, and Cs_2GeNbI_6, as determined by band structure calculations. This is ideal for investigating these compounds for use in solar cells. In addition, the investigated compounds were investigated in terms of optical absorption, refractive index, and dielectric constants for energy range $0-12$ eV, ensuring absorption in infrared, visible, and ultraviolet regions. This was done in order to study optical characteristics. The investigated compounds are excellent candidates for harvest solar cell applications due to their maximum visible absorption. They are also good candidates for thermoelectric applications due to their Seebeck coefficient, lattice thermal, electric conductivities and figure of merit (ZT) addressed by Boltzmann theory.

Keywords: New halide double perovskites; optoelectronic properties; solar cells; direct bandgap semiconductors; thermoelectric applications; density functional theory.

DOI: https://doi.org/10.31349/RevMexFis.69.061001

1. Introduction

Undoubtedly, no one is unaware of the great interest that continues to hover over the studies of perovskite oxides especially since 1993, the year of the discovery of giant magnetoresistance (GMR) in the applications of thin layers of manganese oxides. This is also because of the very wide variety of their properties such as ferroelectricity [1–3], piezoelectricity [4, 5], di-electricity [6, 7], semi-metallicity [8–11], antiferromagnetism [12] coexistence of magnetism and antiferromagnetism [13] and other properties [14–16].

If simple perovskite oxides of general formula ABO_3 do not have good semiconductor properties that make them suitable for photovoltaic (PV) applications, the simple ABC_3 general formula perovskites and even better the $A_2BB'C_6$ general formula perovskites have attracted massive attention due to their unprecedented potential for optoelectronic and thermoelectric applications [17, 21] characterised on the one hand by a gap, remarkable absorption coefficients, a large number of load carriers and an extraordinary optical efficiency [22,23] and on the other hand by the value of the merit factor (ZT) which is the main indicator of thermoelectric performance [24, 25].

These Perovskite materials are also being explored in photovoltaics, which has become a hot and topical research topic in the face of the world energy crisis. Solar energy is currently considered a renewable and alternative energy source because of its clean, non-polluting nature and low operating costs. Even better, the growth in power conversion efficiency (PCE) in perovskite-based solar cells continues to rise according to recent reports, from 3.8 % [26] in 2009 since the first device was launched to nearly 25,7% in 2022 [27–29].

Several classes of perovskite materials have been intensively studied, cited, lead-based halide perovskites that have become excellent semiconductors for a wide range of optoelectronic applications, such as photovoltaic in $CsPbBr_3$ [30], only the presence of lead (Pb) considered as a toxic element in their chemical composition limited their development [31]. This disadvantage is considered to be one of the main factors limiting their marketing. The solution lies in eradicating toxicity by substituting the "Pb" element with other non-toxic elements [32]. In this context, several studies on lead-free perovskites have been initiated, similar to the one on double perovskites $Rb_2AgTlCl_6$ and $Cs_2AgTlCl_6$ by Murtaza *et al.*, [33] in which it reveals high stability and absorption for these materials, only not suitable for photovoltaic applications for the simple reason is that they possess a wide optical gap. On the other hand, the synthesis of certain halogenated perovskites such as Cs_2BiAgI_6, $Cs_2InAgCl_6$ and

$Cs_2BiAgBr_6$ [34–36]revealed that these materials are unsuitable for photovoltaic applications due to their wide gaps and limited optical characteristics.

Several studies have been conducted in the same context but have had the same fate [37–39]. The most promising solution to the problems raised was probably found in Cai *et al*. [40] after studying a series of double halide perovskites without Pb in this case Cs_2GeMX_6 (M = Ti, V, Cr, Mn, Fe, Co, Ni or Cu, X = Cl, Br or I using a DFT calculation by modulating the structures of these materials to obtain small gaps. Indeed, these materials have been promising in showing non-toxic character and structural stability, a great spin separation with a very high Tc predicting their application in spintronics. These same materials have been intensively studied and have proved to be good potential candidates for photovoltaic applications [41].

In the light of the above literature and motivated by these studies, we explored for the first time by an ab-initio calculation, the structural, magnetic, optoelectronic and thermoelectric aspects of the new double perovskite halide Cs_2GeNbX_6 (X = Cl, Br, I) to make them suitable for experimental manufacture of solar cells and possibly adapt them to optoelectronic applications. It should be recalled that niobium is a transition metal with an electronic structure of $(K)^2(L)^8(M)^{18}(N)^{12}(O)^1$. It crystalizes in body-centered cubic (bcc), at room temperature, it is solid, the melting point and the boiling point are respectively 2750 K and 5014 K. It is a silver-Gray metallic chemical element. The steel industry makes use of it. Small amounts of niobium are added to alloys with the goal of making them more resistant to corrosion and high pressures. As a result, Niobium can be found in things like rockets, satellites, high-resistance pipes, and jet planes. Niobium-containing alloys (Niobium-Titanium or Niobium-Tin) are utilized in the production of superconducting magnets and prosthetics in the medical field.

2. Method of calculations

Ab-initio calculations of niobium new halide double perovskites Cs_2GeNbX_6 (X = Cl, Br, I) have been performed within Density Functional Theory (DFT) implemented in the electronic structure calculation code Wien2k (0K, 0 Gpa) [42] based on the hybrid full-potential L/APW+lo method [43].

In this method the unit cell is divided into non-overlapping muffin-tin (MT) spheres, inside of which the basic functions are expanded in spherical harmonics functions and the basic functions in the interstitial region, outside the MT spheres, are plane waves.

The PBE-GGA approximation was used to calculate precise lattice constants, ground state energy and bulk modulus though Murnaghan's equations of states for studied our materials [44–46]. It was used also to calculate optoelectronic and magnetic properties.

To attain excellent convergence, the orbital quantum number l in the atomic sphere waslimited to $l_{\max} = 10$ for wave function derivation, the values correspondingto the largest vector in charge density Fourier expansion (Gmax) and RMT×Kmax were set to 12 and 7 respectively, to separate core states from valence states, the cut-off energy was set to $(-6Ry)$. Moreover, $k-$mesh size in the first Brillouin zone was preferred to be 2500 k$-$ points equivalent to a $13 \times 13 \times 13$ which releases the maximum energy. The energy selected was $0.0001Ry$ during self-consistency cycles. In this work, we have treated the electronic states of Cs ($6s^1$), Ge ($3d^{10}4s^24p^2$), Nb ($4d^4\ 5s^1$), Cl ($3s^2\ 3p^4$), Br ($4s^2\ 3d^{10}4p^5$) and I ($4d^{10}5s^25p^5$) atoms as configurations of the valence states. Finally, the BoltzTrap code [47]is used to compute thermoelectric properties including coefficient of Seebeck (S), electrical conductivity (σ) and figure of Merit (ZT). The lattice thermal conductivity was computed by ShengBTE code [48].

TABLE I. Bond lengths between Cs$-X$, Ge$-X$, Nb$-X$ in ground stable state where $(X =$ Cl, Br, I).

Compound	Bond	Bond length(Å)	Bond length theo.(Å) [41]
$Cs_2GeNbCl_6$	Ge-Cl	2.54	2.53
	Nb-Cl	2.75	2.74
	Cs-Cl	3.75	3.75
$Cs_2GeNbBr_6$	Ge-Cl	2.67	2.66
	Nb-Cl	2.90	2.88
	Cs-Cl	3.94	3.92
Cs_2GeNbI_6	Ge-Cl	2.86	2.86
	Nb-Cl	3.10	3.09
	Cs-Cl	4.025	4.21

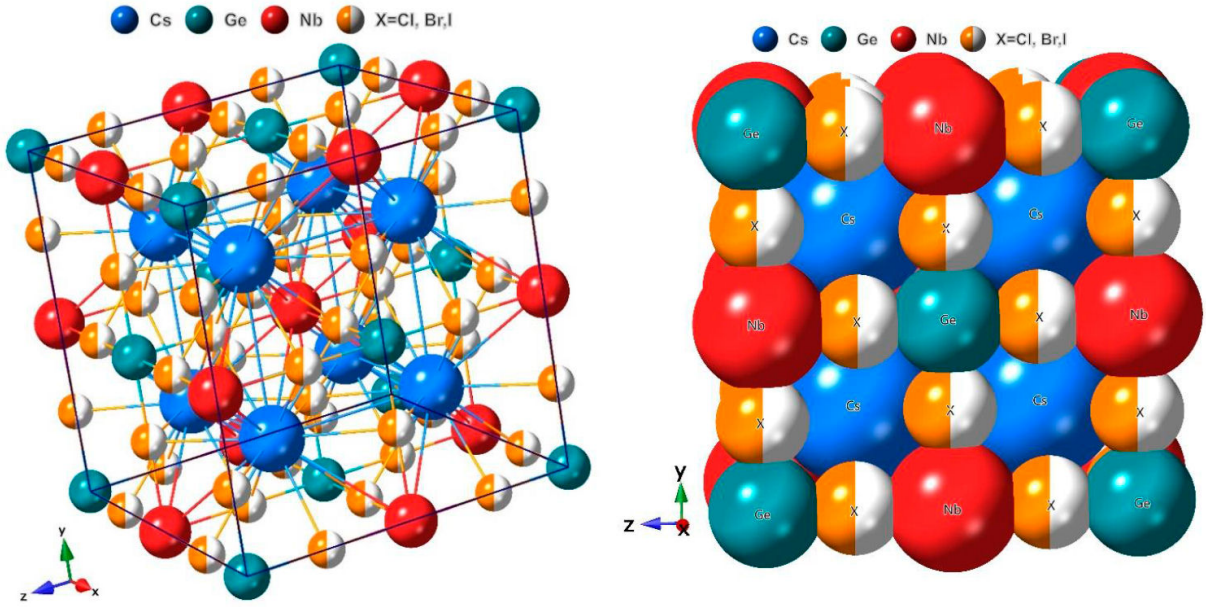

FIGURE 1. a) Cubic crystal structure of niobium new halide double perovskites Cs_2GeNbX_6 (X = Cl, Br, I) in atomic form. b) Cubic crystal structure of niobium new halide double perovskites Cs_2GeNbX_6 (X = Cl, Br, I) in atomic form in front view.

3. Results and discussion

3.1. Structural properties

The cubic niobium new halide double perovskites Cs_2GeNbX_6 (X = Cl, Br, I) system investigated here has face-centered cubic group (Fm-3m). To confirm the stability of our materials in the cubic structure in the ground state, we engaged the tolerance factor "t" of Goldschmidt [49]:

$$t = \frac{r_{Cs} + r_X}{\sqrt{2}\left(\frac{r_{Ge}+r_{Nb}}{2} + r_X\right)}, \quad (1)$$

where r_{Cs} designates the ionic radii of Cs and r_X represents the ionic radii of X =Cl, Br, l while $(r_{Ge} + r_{Nb})/2$ signifies the average of ionic radii of the Ge and Nb. The tolerance factors respectively for Cs_2GeNbX_6 (X = Cl, Br, I) were found at 0.97, 0.95 and 0.93, values belonging to the range $[0.9, 1]$ confirming that our compounds indeed have cubic structures. These cubic crystal structures are illustrated via Fig. 1 where the cubic niobium new halide double perovskites Cs_2GeNbX_6 (X = Cl, Br, I) consists of alternatively arranged four GeX_6 and four NbX_6 octahedrons along the crystallographic axes with Ge and Nb located at the center of GeX_6 and NbX_6 octahedron. They consist also of $3D$ network of corner-sharing halide octahedra with alternating Ge^+ and Nb^{3+} centers, which are filled with Cs ions at octahedral interstice (Fig. 1). It is also observed that the bond length betweenall the atoms is respectively proportional to the size of the halide (Cl, Br, I) (Table I). Our results agree with other [41].

The experimental value of lattice parameter reported by Zeng and al [50] are $a = 10.49$ Å, $a = 11.08$ Åand $a = 11.89$ Å, for respectively Cs_2GeNbX_6 (X = Cl, Br, I). In Wyckoff coordinates [51], the atomic positions are given such Cs in $8c$ at (0.25, 0.25, 0.25); Ge in $4b$ at (0, 0, 0); Nb in $4a$ at (0.5, 0.5, 0.5), and X in $24e$ at (0.24, 0, 0).

The structural parameters are calculated by Murnaghan equation of states [52] to obtain equilibrium lattice constant as the constant a (Å), the bulk modulus B (Gpa), its pressure derivative B' and minimum energy values (E_0) with GGA approach. The structural parameters are tabulated in Table II.

TABLE II. The lattice parameters optimized with GGA for Cs_2GeNbX_6 (X = Cl, Br, I) in comparison with experimental values.

Compound	Config.	a(Å)	a(Å)theo [41]	V(Å)^3	B(GPa)	B'	E_0(eV)
$Cs_2GeNbCl_6$	FM	10.60	10.55	2011.08	28.84	4.56	-660409.35
	NM	10.51	10.48	1959.24	30.07	4.55	-660408.04
$Cs_2GeNbBr_6$	FM	11.08	11.11	2343.72	24.52	4.69	-1010639.40
	NM	11.06	11.04	2282.02	26.13	4.56	-1010638.16
Cs_2GeNbI_6	FM	11.93	11.92	2870.16	19.83	4.58	-1747366.93
	NM	11.81	11.83	2782.42	22.69	3.62	-1747366.84

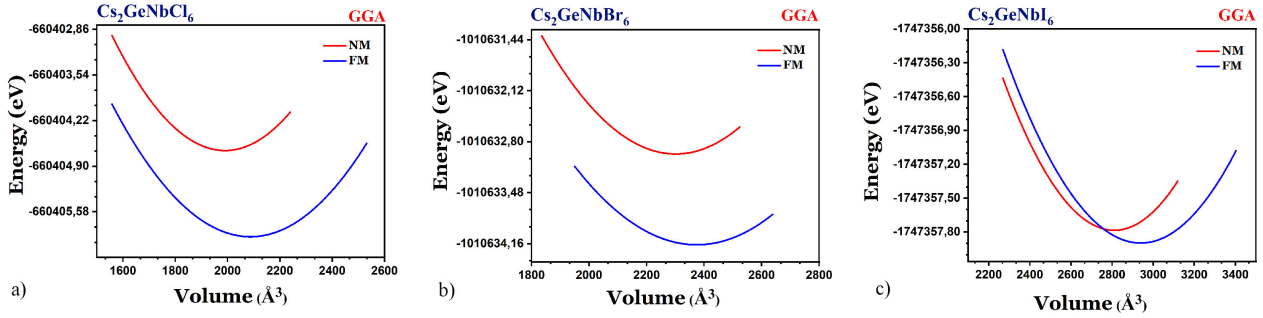

FIGURE 2. Variation of the total energy as a function of the volume for the cubic niobium new halide double perovskites Cs_2GeNbX_6 (X = Cl, Br, I) in non-magnetic and ferromagnetic states using GGA approximations

It can be seen that the lattice parameters calculated from the optimization are in agreement with the theoretical data [41], moreover their values increase when the radii of the halide ions increase from Cl to I, contrariwise, a reverse trend was observed for the case of bulk modulus which shows a decreasing value upon changing halide ions.

Furthermore, we have calculated the GGA total energies in nonmagnetic and magnetic ordering configurations wherefrom it can be concluded that the magnetic state has been taken as reference for its lowest total energy as shown in Figs. 2a)-c).

In summary, the studied niobium new halide double perovskite Cs_2GeNbX_6 (X = Cl, Br, I) structures are stable and can be used for characterization to explore their applications.

3.2. Magnetic properties

Table III includes the results of the spin effect of the magnetic moment of niobium new halide double perovskites Cs_2GeNbX_6 (X = Cl, Br, I) compounds using the GGA approximation.

It summarizes the calculated spin magnetic moments for Cs ($\mu-$Cs), Ge ($\mu-$Ge), Nb($\mu-$Nb), (X = Cl, Br, I) ($\mu-X$), atoms, interstitial region (μ-interst) and cell (μ-Cell.), respectively versus the exchange correlation potential.

The theoretical results [40] are also presented for comparison. The values of the magnetic moments were around 3 μB/atom for niobium new halide double perovskites Cs_2GeNbX_6 (X = Cl, Br, I).

It is clear that the origin of magnetism comes from only the niobium atom (1.22 μB/atom), this is mainly due to the orbitals Nb$-3d$ because in $Cs_2^{1+}Ge^{2+}Nb^{2+}X_6^{1-}$ (X = Cl, Br, I) configuration, only Nb^{2+} sitesown $3d$ unpaired electrons which participate in octahedron crystal field splitting giving origin to the ferromagnetic character of our compounds.

3.3. Electronic properties

A material's various physical properties are heavily influenced by its electronic structures. In order to find smart materials for technological applications, it is therefore necessary to comprehend the structure of spin-polarized band densities and spin polarized band structures [53, 54].

3.3.1. Band structure

Figures 3a)-f) depict the band structures diagram of the niobium new halide double perovskites Cs_2GeNbX_6 (X = Cl, Br, and I) along high-symmetry lines in the cubic Brillouin zone where the energy zero of the band structure diagram has been taken at the Fermi level.

In both spin channels (spin-up and spin-dn), The GGA method shows via Figs. 3a)-f) that conduction band minima and valence band maxima are separated by a direct band gap type at L point in the Brillouin zone justifying the semiconducting nature of our compounds.It is essential to know that the direct band gaps guarantee the inter-band transition when considering applications in optoelectronics and solar cells.

In spin-dn [Figs. 3b), d) and f)], the band gaps for $Cs_2GeNbCl_6$, $Cs_2GeNbBr_6$ and Cs_2GeNbI_6 are found to be 3.14 eV, 2.79 eV, and 2.36 eV, respectively. However, in spin-up [Figs. 3a), c) and e)], the band gaps for the same compounds are found to be much smaller: 0.73, 0.51, and 0.3 eV,

TABLE III. Results of the magnetic moments (in Bohr magneton, μB) of the Cs_2GeNbX_6 (X = Cl, Br, I) using the GGA approximation.

Compound	Magnetic moments(μ_B)						
	μ**Cs**	μ**Ge**	μ**Nb**	μ **X**	μ **interst.**	μ **Cell**	μ **Cell [40]**
$Cs_2GeNbCl_6$	0.00074	−0.006	1.22	0.00383	1.7	3.00131	3
$Cs_2GeNbBr_6$	0.0004	−0.008	1.21	0.00118	1.8	3.0005	3
Cs_2GeNbI_6	−0.00002	−0.007	1.60	−0.00152	1.42	3.0012	3

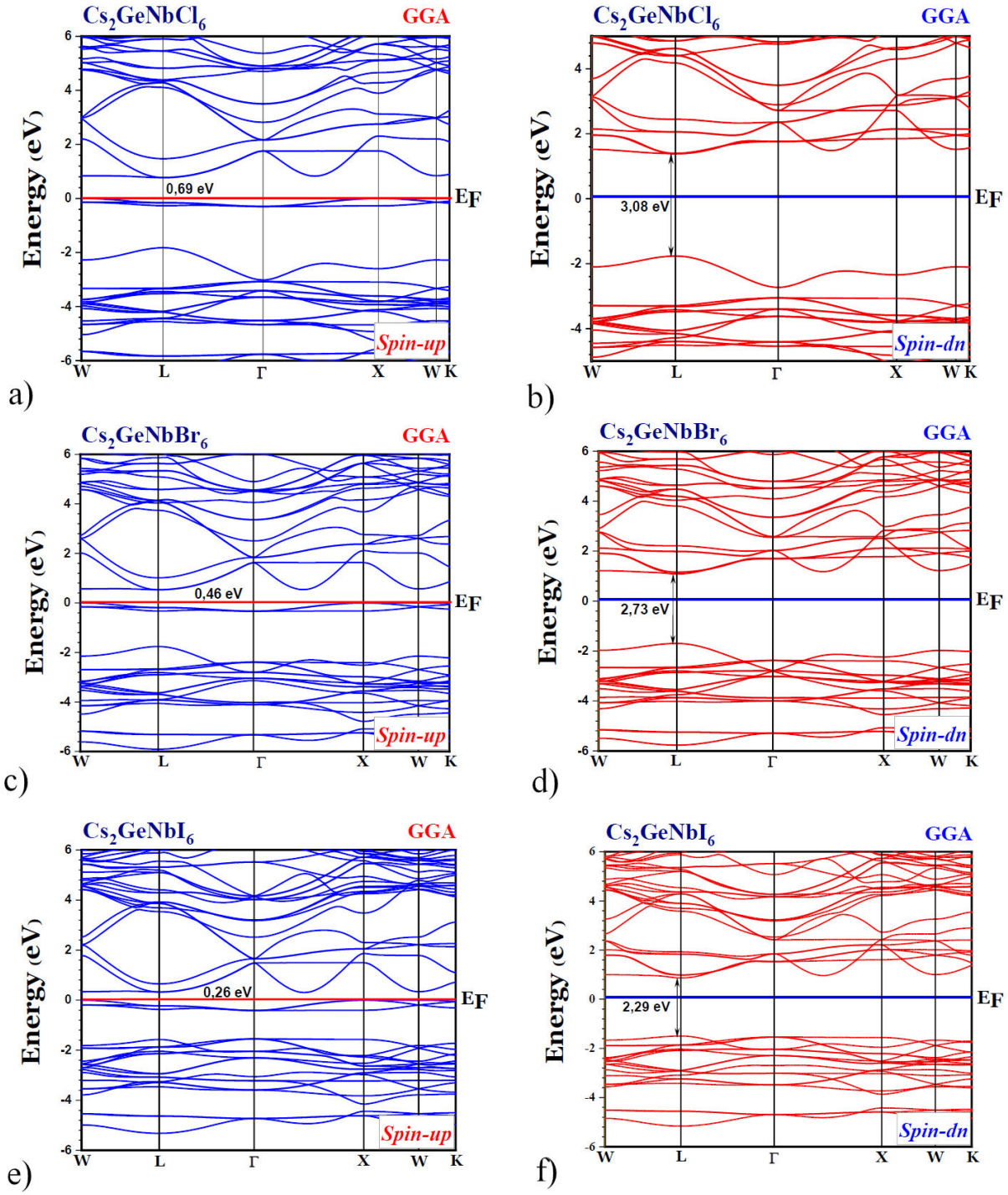

FIGURE 3. The spin-resolved energy bands of niobium new halide double perovskites Cs_2GeNbX_6 (X = Cl, Br, I) via generalized gradient approximation (GGA): figures a), c) and e) represent the spin-up states, figures b), d) and f) represent the spin-dn states, respectively.

respectively. Because of this, their band gaps make them suitable materials for thermoelectric and solar cell applications.

It is obvious that the bandgap shrinks when Cl is replaced by Br and then by I as long as their electronegativity decreases. The gap between the valence band and the conduction band narrows as a result of the states being pushed closer to the Fermi level as anions grow in size. Additionally, the band structure ensures that the number of states in the valence band is significantly higher than in the conduction band. The states are curved in the conduction band and flat

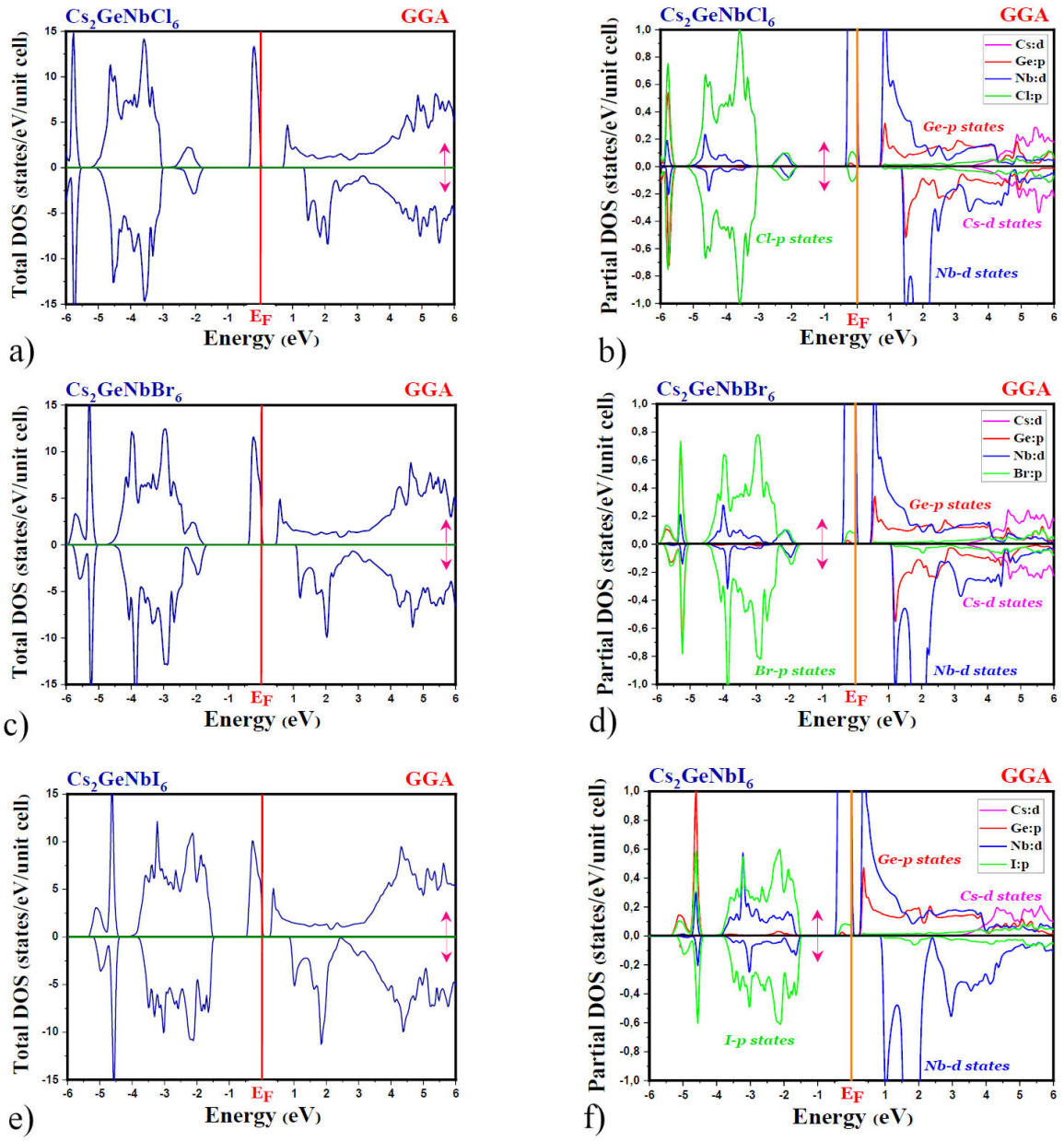

FIGURE 4. The total and partial DOSs plots of niobium new halide double perovskites Cs_2GeNbX_6 (X = Cl, Br, I) via generalized gradient approximation (GGA): figures [a), d)],[b),e)] and [c), f)] represent total and partial Dos of $Cs_2GeNbCl_6$, $Cs_2GeNbBr_6$ and Cs_2GeNbI_6, respectively.

in the valence band. Finally, other halide perovskites exhibit the same band tuning phenomenon as our compounds [55].

3.3.2. *Density of states (DOS)*

Utilizing generalized gradient approximation (GGA), the total and partial DOSs plots of the niobium new halide double perovskites Cs_2GeNbX_6 (X = Cl, Br, and I) are depicted in Fig. 4. The semi-conducting nature of our compounds is also confirmed by these DOS plots. The conduction band is dominated by the $Nb-d$ state and a mixture of Ge$-p$, Cs$-d$, and halogen Cl/Br/I$-p$, while the wide valence bands are dominated by halogen Cl/Br/I$-p$ states with a small role from Ge$-p$ states in the range of -6 to -5 eV. The hybridized orbitals of the Nb$-d$-states, the Ge$-p$-states and the Cl/Br/I$-p$ states, which are thought to contribute the majority of the occupation levels around the Fermi level, are fundamentally responsible for the formation of band gaps in these compounds. At the same time, orbital contributions from the Cl/Br/I$-p$ states most likely populate the core states of the valence band. Finally, we confirm that both spin states exhibit a direct gap around the Fermi level.So, our materials are suitable for photovoltaic applications.

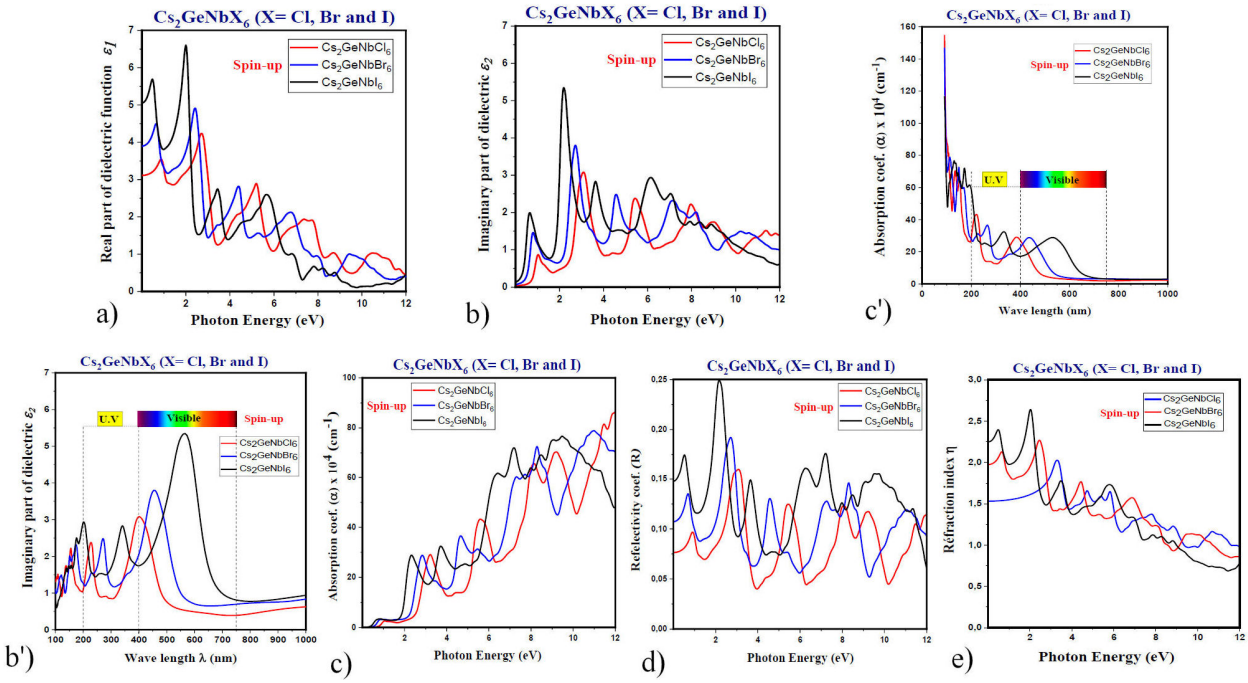

FIGURE 5. The computed optical parameters of niobium new halide double perovskites Cs_2GeNbX_6 (X = Cl, Br, and I) calculated with GGA: a) real part of dielectric function $\epsilon_1(\omega)$, b) imaginary part of dielectric function $\epsilon_2(\omega)$, c) absorption coefficient $\alpha(\omega)$, d) reflectivity $R(\omega)$ and e) refractive index $n(\omega)$.

3.4. Optical properties

In order to determine the efficiency of photovoltaic devices and investigate their suitability for solar applications, research into optical spectroscopy analysis [56, 57] is crucial. Our niobium new halide double perovskites Cs_2GeNbX_6 (X = Cl, Br and I) have a greater potential for optoelectronic and solar cell applications due to their direct small band gaps [58] where energy absorption maximum incident occurs in this region.

The computed optical parameters of the niobium new halide double perovskites Cs_2GeNbX_6 (X = Cl, Br, and I) using GGA along the xx axes are depicted in Fig. 5. These optical parameters include real part of dielectric function $\epsilon_1(\omega)$, imaginary part of dielectric function $\epsilon_2(\omega)$, absorption coefficient $\alpha(\omega)$, reflectivity $R(\omega)$ and refractive index $n(\omega)$.

The complex dielectric function $\epsilon(\omega)$ is regarded as the most significant measurable optical quantity because all the other optical constants are derived from it. It is given by the relation:

$$\epsilon(\omega) = \epsilon_1(\omega) + i\epsilon_2(\omega), \tag{2}$$

where $\epsilon_1(\omega)$ represents the real and $\epsilon_2(\omega)$ the imaginary parts [59, 60]. Calculations of the electronic dielectric function spectra (Fig. 5) are carried out for energy radiation above the Fermi level in the range of $0 - 12$ eV.

- The real part of the dielectric function $\epsilon_1(\omega)$ [Fig. 5a)] explains widely the electronic polarizability of a compound as a response to electromagnetic wave interactions.

For $Cs_2GeNbCl_6$, $Cs_2GeNbBr_6$, and Cs_2GeNbI_6, the real part's static dielectric constant yields values of 3.50, 4.46, and 5.68, respectively. According to Penn's relation [61], these static values have an inverse relationship with band gaps of 0.73 eV, 0.51 eV, and 0.3 eV, respectively. In addition, the graph demonstrates that $\epsilon_1(\omega)$, initially exhibited peaks of polarized lights at 2.71 eV, 2.38 eV, and 1.99 eV for $Cs_2GeNbCl_6$, $Cs_2GeNbBr_6$, and Cs_2GeNbI_6, respectively, before beginning to decrease. The resonance frequency is clearly fully polarized in a direction perpendicular to the electric field of the incident light from the peak intensities. Moreover, after a cation replacement from Cl to I passing through Br, it moves toward lower photon energy. In addition, the peaks began to decrease to a minimum value over the resonance, but they remained positive for all of the compounds we studied, indicating that these materials remained polarized and exhibited semiconducting behavior.

- Figure 5b) of the niobium new halide double perovskites Cs_2GeNbX_6 (X = Cl, Br, and I) shows the imaginary segment of the dielectric constant "$\epsilon_2(\omega)$" that represents the absorption of light. The optical gaps of $Cs_2GeNbCl_6$, $Cs_2GeNbBr_6$ and Cs_2GeNbI_6 are represented by threshold energies of 0.69, 0.46, and 0.26 eV, respectively. These values are consistent with band gaps calculated from band structure, ensuring the accuracy of theoretical band structure and optical analysis calculations made with GGA.

$Cs_2GeNbCl_6$, $Cs_2GeNbBr_6$ and Cs_2GeNbI_6 exhibit distinct prominent peaks (3.00, 3.81 and 5.35) at energies of 3.20 eV, 2.74 eV, and 2.20 eV, respectively, for the investigated compound Cs_2GeNbX_6 (X = Cl, Br, and I). Direct electron transfer from valence band states to conduction band

TABLE IV. The absorption bands of light for Cs_2GeNbX_6 (X = Cl, Br, I).

Compound	**Ultraviolets**		**Visible**
	Range 1 [λ (nm)]	**Range 2** [λ (nm)]	**Range 3** [λ (nm)]
$Cs_2GeNbCl_6$	$200-257$	$310-400$	$400-500$
$Cs_2GeNbBr_6$	$200-300$	$343-400$	$400-600$
Cs_2GeNbI_6	$200-230$	$293-400$	$400-750$

states is what causes these peaks. For the Cs_2GeNbX_6 ($X =$ Cl, Br, and I) compound under investigation, the shifting of absorption bands towards lower energy from visible to infrared region is because of replacement of Cl with Br and I. This is consistent with the pattern that was observed for the TDOS, where a smaller bandgap was observed when X switched from Cl to Br and I. The studied materials, on the other hand, have the majority of their absorption in the visible and ultraviolet regions [Fig. 5b)] making them excellent materials for solar cells and optoelectronic devices [Table IV].

-The performance of solar energy conversion by solar cells is dynamically determined by the optical absorption coefficient, which is dependent on the material's ability to harvest light. The studied Cs_2GeNbX_6 ($X =$ Cl, Br, and I) compounds' absorption coefficients $\alpha(\omega)$ are shown in Figs. 5c) and c') and reveal that they do not absorb light below the band gap values due to the collision between electrons and photons. When halide ions switched from Cl to Br and I, respectively, $\alpha(\omega)$ splits in various values and began shifting toward lower energy. The semiconducting nature of the investigated compounds is demonstrated by the linearly increasing trend in absorption after passing limiting energy. The absorption bands of the imaginary segment of the dielectric constant $\epsilon_2(\omega)$ and $\alpha(\omega)$ are consistent.

-Light reflection, denoted by $R(\omega)$ in Fig. 5d), can be used to investigate the computed materials' surface morphology. $Cs_2GeNbCl_6$, $Cs_2GeNbBr_6$, and Cs_2GeNbI_6's $R(\omega)$ values at zero photon energy were approximately 0.076, 0.108, and 0.147, respectively. $R(\omega)$ for $Cs_2GeNbCl_6$, $Cs_2GeNbBr_6$, and Cs_2GeNbI_6 reaches maximum values of 0.16 at 3.06 eV, 0.19 at 2.69 eV, and 0.25 at 2.21 eV as photon energy increases. These materials' low and high reflectivity values demonstrate that they absorb a lot of electromagnetic energy in the low energy range. As a result, we can say that Cs_2GeNbX_6 ($X =$ Cl, Br, and I) is a best material for photovoltaic and optoelectronic applications like LEDs and solar cells.

- Figure 5e) depicts the refractive index values $n(\omega)$, which provide estimates of the material's density and light speed dependence. Using [Fig. 5e)], it stands to reason that $n(\omega)$ and $\epsilon_1(\omega)$ [Fig. 5a)] display a dispersion curve that is very similar, demonstrating that the spectra that correspond to the refractive index are very similar to the spectra of the real segment of the dielectric constant. From these spectra, we can calculate the static refractive index by using the equation $n(0) = [1(0)]^{1/2}$ [62, 63]. The static refractive index values for $Cs_2GeNbCl_6$, $Cs_2GeNbBr_6$, and Cs_2GeNbI_6 were found to be 1.76, 1.98 and 2.25. They were the same values that were taken from Fig. 5a). Additionally, the maximum values of $n(\omega)$ for $Cs_2GeNbCl_6$, $Cs_2GeNbBr_6$, and Cs_2GeNbI_6 at energies above the zero-frequency value are 2.03 at 3.28 eV, 2.26 at 2.45 eV, and 2.66 at 1.98 eV, respectively. The $n(\omega)$ was moved to higher intensity and lower energy when Cl was replaced by Br and I. Solar cells are better suited to the $n(\omega)$ range of 1.4 to 3.87.

3.5. Thermoelectric performances

The direct conversion of heat into electricity (Seebeck effect), electricity into heat (Peltier effect), or conductor heating/cooling (Thomson effect) is known as thermoelectricity. It is also referred to as the Peltier-Seebeck effect. The potential gradient, lattice vibration, and the carriers in the material's structure all play a role in the thermoelectricity properties. The thermoelectric properties of the niobium new halide double perovskites Cs_2GeNbX_6 (X = Cl, Br, and I) at temperatures $T(K)$ and chemical potential (eV) were calculated using the BoltzTraP code [47].

We have characterized our studied compounds for their thermoelectric performance from figure of merit (ZT) as given by ZT $= (\sigma S^2/\kappa T)$ [64–66] where κ denotes electrons thermal conductivity, S Seebeck coefficient, σ indicate the electrical conductivity and T is the kelvin temperature. It has been discovered that the band gaps and electronic behavior have a significant impact on the thermoelectric properties, and the trends are investigated in relation to increasing temperatures between 200 and 600 K. The thermoelectric applications of the narrow band gap materials are thought to be promising. Electrons easily move from valence to conduction bands in semiconductors with a narrow band gap, which improves electrical conductivity and decreases thermal conductivity. Figures 6a)-d) depicts the Seebeck coefficient (S), electrical conductivity (σ), thermal conductivity (κ) and the thermoelectric efficiency (ZT) of the niobium new halide double perovskites Cs_2GeNbX_6 (X = Cl, Br, and I).

- Figure 6a) shows the calculated Seebeck coefficient S, which indicates the potential difference between two metal connections over a temperature gradient ΔT. With p-type behavior, it gradually decreases from 0.18, 0.18, and 0.20 mV/K to 0.14, 0.15 and 0.16 mV/K for Cs_2GeNbX_6, $Cs_2GeNbBr_6$, and Cs_2GeNbI_6, respectively, over a broad temperature range of 200 to 600 K. It is important to note

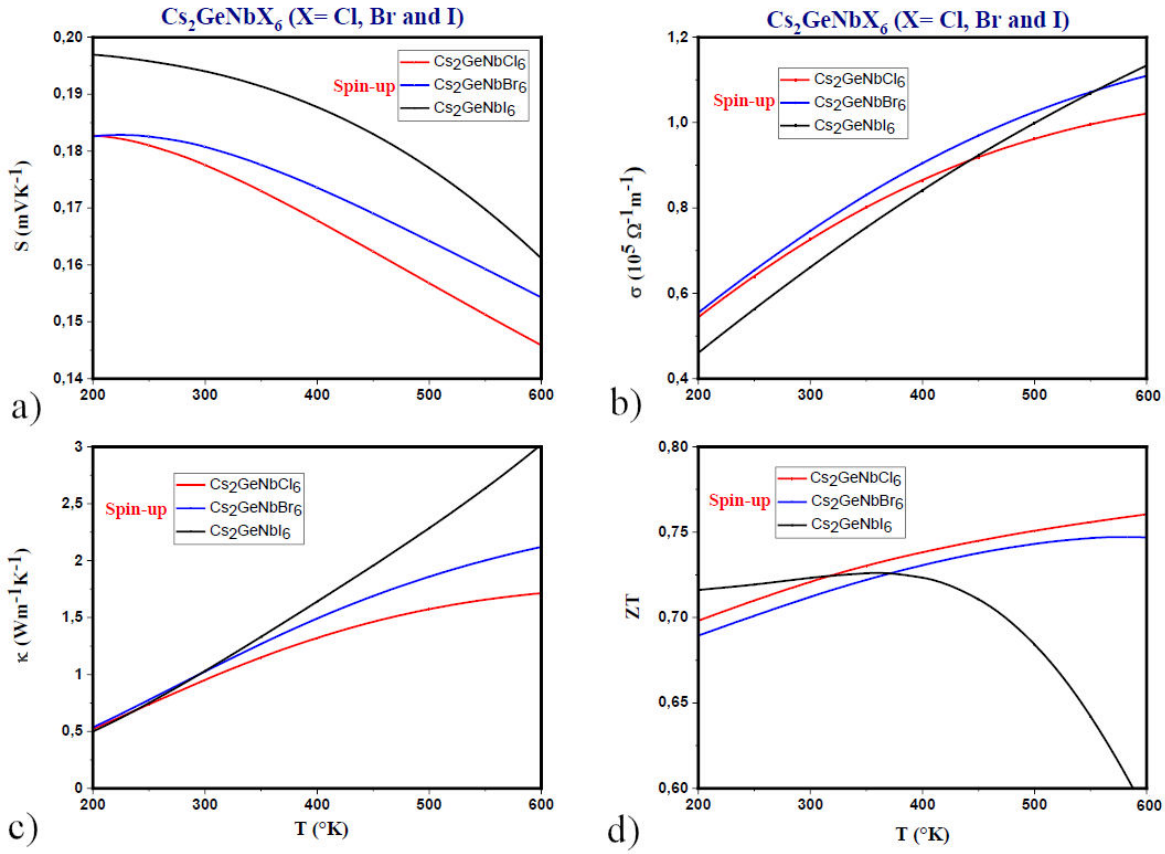

FIGURE 6. The temperature dependence of the calculated a) Seebeck coefficient (S), b) electrical conductivity over relaxation time (σ/τ), c) thermal conductivity (κ) and d) the thermoelectric efficiency (ZT) of the niobium new halide double perovskites Cs_2GeNbX_6 (X = Cl, Br, and I).

that the Seebeck coefficient S for $Cs_2GeNbCl_6$, $Cs_2GeNbBr_6$, and Cs_2GeNbI_6 was found to be 0.17, 0.18, and 0.19 mV/K at room temperature, respectively. These values indicate that S increases when Cl is replaced by Br and then by I.

- Figure 6b), the electrical conductivity (σ) against temperature was shown to increase with temperature. This raises the electron conduction of the studied compounds, possibly as a result of bond breaking and the high kinetic energy of electrons. This also indicates the existence of an energy gap close to the Fermi level. At 200 K, the electrical conductivity (σ) values of $Cs_2GeNbCl_6$, $Cs_2GeNbBr_6$, and Cs_2GeNbI_6 reach their highest values of 1.02, 1.10, and 1.13×10^6 $\Omega^{-1}m^{-1}$ at 600 K when the minimum values werefound to be 0.54, 0.55 and 0.46×10^6 $\Omega^{-1}m^{-1}$ at 200 K, respectively. This outcome is extremely satisfying; As a result, we can speculate that the computed materials represent a promising candidate for applications in thermoelectric technology.

- Figure 6c) shows the calculated thermal conductivity (κ) for Cs_2GeNbX_6 (X = Cl, Br, and I) as a function of $T(K)$. For $Cs_2GeNbCl_6$, $Cs_2GeNbBr_6$, and Cs_2GeNbI_6, the (κ) rises from 0.52, 0.52, and 0.52 W/mK at 50 K to 1.71, 2.12, and 3.00 W/mK at 600 K, respectively. However, the fact that the (κ) is 105 times smaller than highlights the potential applications of the investigated materials for solar cells [67].

- For the accurate and complete judgement of performance of thermoelectric devices, ZT values are presented in Fig. 6d) for T. When ZT is plotted in the temperature range of $200 - 600$ K, ZT rises from 0.70 and 0.69 to 0.76 and 0.75 for $Cs_2GeNbCl_6$ and $Cs_2GeNbBr_6$, respectively. At room temperature, the studied Cs_2GeNbI_6 has a ZT of 0.72. Due to these properties, our studied compounds are suitable for thermoelectric applications.

4. Conclusion

The Wien2k package's ab-initio full potential linear augmented plane wave (FP-LAPW) method was used to calculate structural, magnetic, electronic, optical, and thermoelectric properties of the niobium new halide double perovskites Cs_2GeNbX_6 (X = Cl, Br, and I). In the framework of Perdew-Burke-Ernzerh (PBE), the generalized gradient approximation (GGA) was utilized to handle the exchange correlation potential. The thermoelectric properties were also calculated using the BoltzTrap code.

The tolerance factor of Goldschmidt confirmed that the investigated compounds stabilize in a cubic struc-

ture.Moreover, they were found to be ferromagnetic and have high magnetic moments of more 3 μB. The band structure and DOS revealed that Cs_2GeNbX_6 (X = Cl, Br, and I) has a semiconducting behavior with a narrow direct band gap in the spin up state with values of 0.69, 0.46, and 0.26 eV. As a result, these materials are suitable for use in optoelectronics and solar cells.

The investigated materials have the highest absorption rates of both visible and ultraviolet light. In addition, when Br and I were used in place of Cl, their refractive index $n(\omega)$ increased to a higher value at a lower energy, making them excellent materials for solar cells and optoelectronic devices.

These materials are also suitable for thermoelectric applications due to their high ZT values in the temperature range of 200-600 K and their high electrical conductivity despite their low thermal conductivity.

As a result, the experimental community will benefit greatly from the aforementioned the niobium new halide double perovskites Cs_2GeNbX_6 (X = Cl, Br, and I)' findings regarding their potential to boost the solar cells and thermoelectric generators industries.

1. J. F. Scott and M. Dawber, Oxygen-vacancy ordering as a fatigue mechanism in perovskite ferroelectrics, *Appl. Phys. Lett.* **76** (2000) 3803, https://doi.org/10.1063/1.126786.
2. J. J. Urban, W. S. Yun, Q. Gu and H. Park, Synthesis of single-crystalline perovskite nanorods composed of barium titanate and strontium titanate, *J. Am. Chem. Soc*. **124** (2002) 1187, https://doi.org/10.1021/ja017694b.
3. M. Tyunina *et al*., Perovskite ferroelectric tuned by thermal strain, *Sci. Rep.* **9** (2019) 3677, https://doi.org/10.1038/s41598-019-40260-y.
4. S. A. Khan *et al.*, Piezoelectric and ferroelectric properties of lead-free Ga-modified 0.65$BiFe_{O3}$-0.35$BaTiO_3$ ceramics by water quenching process, *Ferroelectrics* **541**(2019) 60, https://doi.org/10.1080/00150193.2019.1574642.
5. R. Song *et al*., High Temperature Stability and Mechanical Quality Factor of Donor-Acceptor Co-Doped BaTiO3 Piezoelectrics, *SSRN Electronic Journal* **3406952** (2019), https://doi.org/10.2139/SSRN.3406952.
6. B. Garbarz-Glos, W. Bak, A. Kalvane, M. Antonova and G. Klimkowski, Effects of CuO doping on structure, microstructure and dielectric properties of BaTiO3-PbTiO3 solid solution, *Integrated Ferroelectrics* **196** (2019) 77, https://doi.org/10.1080/10584587.2019.1591961.
7. R. Gotardo *et al.*, Dielectric, magnetic and structural characterizations in Mn doped 0.9 BiFeO3-0.1 BaTiO3 compositions, *Ferroelectrics* **534** (2018) 102, https://doi.org/10.1080/00150193.2018.1471950.
8. B. Bouadjemi, S. Bentata, A. Abbad, W. Benstaali and B. Bouhafs, Half-metallic ferromagnetism in PrMnO3 perovskite from first principles calculations, *Solid State Commun*. **168** (2013) 10, https://doi.org/10.1016/j.ssc.2013.06.008.
9. G. Chen, C. Dai, and C. Ma, A stable half-metallic ferromagnetic material SrNiO3: a prediction from first principles, International Conference on Mechatronics, Electronic, *Industrial and Control Engineering* (MEIC-14) (2014), https://doi.org/10.2991/meic-14.2014.167.
10. A. Sajawal, M. Ishfaq, G. Murtaza, I. Habib, N. Muhammad, and S. Sharif, Half metallic ferromagnetism in PrMnO3 orthorhombic stable phase: an experimental and theoretical investigation, *Mater. Res. Express* **5** (2018) 116103, https://doi.org/10.1088/2053-1591/aade7d.
11. A. Labdelli, A. Boukortt, S. Meskine, H. Abbassa, and A. Zaoui, Investigation of optoelectronic and thermoelectric properties of half-metallic BaRuO3 using DFT+U, *Int. J. Comput. Mater. Sci. Eng.* **7** (2018) 1850018, https://doi.org/10.1142/S2047684118500185.
12. A. Labdelli, S. Meskine, A. Boukortt, and R. Khenata, Optoelectronic and magnetic properties of the ortho-perovskite GdRuO3 using DFT+U with spin orbit coupling: predictive study, *J. New Technol. Mater.* **8** (2018) 138, https://doi.org/10.12816/0048932.
13. A. Labdelli and N. Hamdad, Predictive study of ferromagnetism and antiferromagnetism coexistence in $Ba_{1-x}Gd_xRuO_3$ induced by Gd-doping, *Rev. Mex. Fis.* **67** (2021) 8, https://doi.org/10.31349/RevMexFis.67.061002.
14. S.B. Krupanidhi, Ferroelectric thin films and device applications, in: Multicomponent and Multilayered Thin Films for Advanced Microtechnologies: Techniques, Fundamentals and Devices, *Springer* (1993) 625, https://doi.org/10.1007/978-94-011-1727-2_36.
15. R. Waser, Modeling of electroceramics-applications and prospects, *J. Eur. Ceram. Soc.* **19** (1999) 664, https://doi.org/10.1016/S0955-2219(98)00293-3.
16. N. Setter, Electroceramics: looking ahead, *J. Eur. Ceram. Soc.* **21** (2001) 1279, https://doi.org/10.1016/S0955-2219(01)00217-5.
17. E. Greul, M. L. Petrus, A. Binek, P. Docampo and T. Bein, highly stable, phase Pure Cs2AgBiBr6 double perovskite thin films for optoelectronic applications. *J. Mater. Chem.* **5** (2017)19972, https://doi.org/10.1039/C7TA06816F.
18. M. Saxena, K. Tanwar and T. Maiti, environmentally friendly Sr2TiMoO6 double perovskite for high temperature thermoelectric applications, *Scripta Mater* **130** (2017) 205, https://doi.org/10.1016/j.scriptamat.2016.11.033.
19. T. Wu *et al*., Lead-free tin perovskite solar cells, *Joule* **5** (2021) 863, https://doi.org/10.1016/j.joule.2021.03.001.

20. J. S. Manser, J. A. Christians and P. V. Kamat, Intriguing optoelectronic properties of metal halide perovskites, *Chem. Rev.* **116** (2016) 12956, https://doi.org/10.1021/acs.chemrev.6b00136.

21. H. Wang, W. Su, J. Liu and C. Wang, Recent development of n-type perovskite thermoelectric, *J. Materiomics*, **2** (2016) 225, https://doi.org/10.1016/j.jmat.2016.06.005.

22. P.A. Nawaz *et al*., Theoretical investigations of optoelectronic and transport properties of Rb2YInX6 (X= Cl, Br, I) double perovskite materials for solar cell applications, *Sol. Energy* **231** (2022) 586, https://doi.org/10.1016/j.solener.2021.11.076.

23. T. Zelai *et al.*, First-principles study of lead-free double perovskites Ga2PdX6 (X= Cl, Br, and I) for solar cells and renewable energy, *J. Mater. Res. Technol*. **16** (2022), https://doi.org/10.1016/j.jmrt.2021.12.002.

24. S. Mitra, Y. Pak, N. Alaal, M.N. Hedhili, D.R. Almalawi and N. Alwadai, Novel P-type wide bandgap manganese oxide quantum dots operating at deep UV range for optoelectronic, *Adv. Opt. Mater.* **7** (2019) 1900801, https://doi.org/10.1002/adom.201900801.

25. M. W. Mukhtar *et al.*, New lead-free double perovskites A2NaInI6 (A= Cs, Rb) for solar cells and renewable energy; first principles analysis, *Mater. Sci. Eng. B* **273** (2021) 115420, https://doi.org/10.1016/j.mseb.2021.115420.

26. A. Kojima, K. Teshima, Y. Shirai and T. Miyasaka, Organometal halide perovskites as visible-light sensitizers for photovoltaic cells, *J. Am. Chem. Soc*. **131** (2009) 6050, https://doi.org/10.1021/ja809598r.

27. M. Houari *et al.*, Structural, electronic and optical properties of cubic fluoroelpasolite Cs2NaYF6 by density functional theory, *Chin. J. Phys*. **56** (2018) 1756, https://doi.org/10.1016/j.cjph.2018.05.004.

28. X. Xu, Y. Zhong and Z. Shao, Double Perovskites in Catalysis, Electrocatalysis, and Photo(electro) catalysis, *Trends in Chemistry* **1** (2019) 410, https://doi.org/10.1016/j.trechm.2019.05.006.

29. X. Du, D. He, H. Mei, Y. Zhong and N. Cheng, Insights on electronic structures, elastic features and optical properties of mixed-valence double perovskites Cs2Au2X6 (X=F, Cl, Br, I), *Physics Letters* **A384** (2020) 126169, https://doi.org/10.1016/j.physleta.2019.126169.

30. X. Liu, J. Gao and Q. Wang, Structural-property correlations of all-inorganic CsPbBr3 perovskites via synergetic controls by PbBr2, 2-mercapto-3-methyl-4-thiazoleacetic acid and water, *Chem. Eng. J.* **428** (2022) 131117, https://doi.org/10.1016/j.cej.2021.131117.

31. A. Babayigit, A. Ethirajan, M. Muller and B. Conings, Toxicity of organometal halide perovskite solar cells, *Nat Mater.* **15** (2016) 247, https://doi.org/10.1038/nmat4572.

32. V. T. Tiong *et al.*, Octadecylamine functionalized single-walled carbon nanotubes for facilitating the formation of a monolithic perovskite layer and stable solar cells, *Adv. Funct. Mater.* **28** (2018) 1705545, https://doi.org/10.1002/adfm.201705545.

33. G. Murtaza *et al*., Lead Free Double Perovsites Halides X2AgTlCl6 (X = Rb, Cs) for solar cells and renewable energy applications, *J. Solid State Chem.* **297**, (2021) 121988, https://doi.org/10.1016/j.jssc.2021.121988.

34. G. Volonakis *et al*., Lead-free halide double perovskites via heterovalent substitution of noble metals, *J. Phys. Chem. Lett.* **7** (2016) 1254, https://doi.org/10.1021/acs.jpclett.6b00376.

35. A.H. Slavney, T. Hu, A. M. Lindenberg and H.I. Karunadasa, A bismuth-halide double perovskite with long carrier recombination lifetime for photovoltaic applications, *J. Am. Chem. Soc.* **138** (2016) 2138, https://doi.org/10.1021/jacs.5b13294.

36. G. Volonakis *et al*., Cs_2InAgC_{l6}: a new lead-free halide double perovskite with direct band gap, *J. Phys. Chem. Lett.* **8** (2017) 772, https://doi.org/10.1021/acs.jpclett.6b02682.

37. B. Yang *et al*., Lead-free silver-bismuth halide double perovskite nanocrystals, *Angew. Chem.* **130** (2018) 5457, https://doi.org/10.1002/anie.201800660.

38. G. Volonakis, A. A. Haghighirad, H.J. Snaith and F. Giustino, Route to stable lead-free double perovskites with the electronic structure of CH3NH3PbI3: a case for mixed-catio [Cs/CH3NH3/CH(NH2)2]2InBiBr6, *J. Phys. Chem. Lett*. **8**(2017) 3917, https://doi.org/10.1021/ACS.JPCLETT.7B01584.

39. W. Meng, X. Wang, Z. Xiao, J. Wang, D.B. Mitzi and Y. Yan, Parity-forbidden transitions and their impact on the optical absorption properties of lead-free metal halide perovskites and double perovskites, *J. Phys. Chem. Lett.* **8** (2017) 2999, https://doi.org/10.1021/acs.jpclett.7b01042.

40. B. Cai et al., A class of Pb-free double perovskite halide semiconductors with intrinsic ferromagnetism, large spin splitting and high Curie temperature, *Mater. Horiz.* **5** (2018) 961, https://doi.org/10.1039/C8MH00590G.

41. M. Nabi and D. C. Gupta, Small-band gap halide double perovskite for optoelectronic properties, *Int J Energy Res.* **45** (2021) 7222, https://doi.org/10.1002/ER.6307.

42. P. Blaha, K. Schwarz, G. Madsen, D. Kvasnicka, J. Luitz and G. K. H. Madsen, WIEN2k An Augmented Plane Wave Plus Local Orbitals Program for Calculating Crystal Properties User's Guide, WIEN2k 17.1 (Release 07/03/2017) WIEN2k An Augmented Plane Wave + Local Orbitals Program for Calculating Crystal Properties

43. E. Sjöstedt, L. Nordström, and D. Singh, an alternative way of linearizing the augmented plane-wave method, *Solid State Commun.* **114** (2000), https://doi.org/10.1016/S0038-1098(99)00577-3.

44. M. Petersen, F. Wagner, L. Hufnagel, M. Scheffler, P. Blaha and K. Schwarz, Improving the efficiency of FP-LAPW calculations, *Comput. Phys. Commun*. **126** (2000) 294, https://doi.org/10.1016/S0010-4655(99)00495-6.

45. J. P. Perdew *et al.*, Restoring the Density-Gradient Expansion for Exchange in Solids and Surfaces, *Phys. Rev. Lett*. **102** (2009) 039902, https://doi.org/10.1103/PHYSREVLETT.100.136406/FIGURES/2/MEDIUM.

46. J. P. Perdew, K. Burke and M. Ernzerhof, Generalized Gradient Approximation Made Simple, *Phys. Rev. Lett.* **77** (1996) 3865, https://doi.org/10.1103/PhysRevLett.77.3865.

47. G. K. Madsen and D. J. Singh, BoltzTraP. A code for calculating band-structure dependent quantities, *Comput. Phys. Commun*. **175** (2006) 67, https://doi.org/10.1016/j.cpc.2006.03.007.

48. W. Li, J. Carrete, N. A. Katcho and N. Mingo, ShengBTE: A Solver of the Boltzmann Transport Equation for Phonons, *Comput. Phys. Commun.* **185** (2014) 1747, https://doi.org/10.1016/j.cpc.2014.02.015.

49. C. J. Bartel *et al*., New tolerance factor to predict the stability of perovskite oxides and halides, *Science Advances*, **5** (2019) 0693, https://doi.org/10.1126/SCIADV.AAV0693/SUPPL_FILE/AAV0693_TABLE_S4.CSV.

50. B. Cai *et al*., A class of Pb-free double Perovskite halide semiconductors with intrinsic ferromagnetism, large spin splitting and high curie temperature. *Mater. Horiz.* **5** (2018) 961, https://doi.org/10.1039/C8MH00590G.

51. D.-M. Han, X.-J. Liu, S.-H. Lv, H.-P Li, and J. Meng, Elastic properties of cubic perovskite BaRuO3 from first-principles calculations, *Phys. B Condens. Matter.* **405** (2010) 3117, https://doi.org/10.1016/J.PHYSB.2010.04.025.

52. F. D. Murnaghan, The compressibility of media under extreme pressures, Proc. Natl. Acad. Sci. **30** (1944) 244, https://doi.org/10.1073/pnas.30.9.244.

53. S. A. Mir and D. C. Gupta, Understanding the origin of half-metallicity and thermophysical properties of ductile La2CuMnO6 double perovskite, *Int. J. Energy Res.* **43** (2019) 4783, https://doi.org/10.1002/er.4620.

54. T. M. Bhat and D. C. Gupta, Robust thermoelectric performance and high spin polarization in CoMnTiAl and FeMnTiAlcompounds. *RSC. Adv.* **6** (2016) 80302, https://doi.org/10.1039/C6RA18934B.

55. S. Al-Qaisi *et al.*, Tuning of band gap by variation of halide ions in K2CuSbX6 (X = Cl, Br, I) for solar cells and thermoelectric applications, *J. Phys Chem Solids* **174** (2023) 111184, https://doi.org/10.1016/j.jpcs.2022.111184.

56. B. Amin, R. Khenata, A. Bouhemadou, I. Ahmad and M. Maqbool, Optoelectronic response of spinels MgAl2O4 and MgGa2O4 through modified Becke- Johnson exchanges potential, *Phys. B Condens. Matter.* **407** (2012) 2588, https://doi.org/10.1016/j.physb.2012.03.075.

57. M. Maqbool, B. Amin and I. Ahmad, Bandgap investigations and the effect of the In and Al concentration on the optical properties of InxAl1-xN, *J. Opt. Soc. Am. B.* **26** (2009) 2181, https://doi.org/10.1364/JOSAB.26.002181.

58. Z. Xiao, H. Lei, X. Zhang, Y. Zhou, H. Hosono and T. Kamiya, Ligand-hole in [SnI6] unit and origin of band gap in photovoltaic perovskite variant Cs2SnI6, *Bulletin of the Chemical Society of Japan* **88** (2015) 1250, https://doi.org/10.1246/bcsj.20150110

59. A. A. AlObaid *et al*., New lead-free double perovskites (Rb2GeCl/Br)6; a promising material for renewable energy applications, *Mater. Chem. Phys.* **271** (2021), 124876, https://doi.org/10.1016/j.matchemphys.2021.124876.

60. M. M. Al-Anazy *et al.*, Study of optoelectronic and thermoelectric properties of double perovskites for renewable energy, *Physica Scripta* **96** (2021) 125828,https://doi.org/10.1088/1402-4896/AC297A.

61. D. R. Penn, Wave-Number-Dependent Dielectric Function of Semiconductors, *Phys. Rev.* **128** (1962) 2093, https://doi.org/10.1103/PhysRev.128.2093.

62. N. A. Noor, Q. Mahmood, M. Rashid, B. U. Haq and A. Laref, the pressure induced mechanical and optoelectronic behavior of cubic perovskite PbSnO3 via abinitio investigation, *Ceramics International* **44** (2018) 13750, https://doi.org/10.1016/j.ceramint.2018.04.217.

63. M. G. B. Ashiq *et al*., The study of electronics, optoelectronics, thermoelectric, and mechanical properties of Zn/CdSnO3 perovskites, *Materials Science in Semiconductor Processing* **137** (2022) 106229, https://doi.org/10.1016/j.mssp.2021.106229.

64. H.C. Wang, P. Pistor, M. A. L. Marques and S. Botti, Double perovskites as p-type conducting transparent semiconductors: a high-throughput search, *J. Mater Chem A.* **7** (2019) 14705,https://doi.org/10.1039/C9TA01456J.

65. Q. Mahmood *et al.*, First-principles study of lead-free double perovskites K2Pt (Cl/Br)6 for optoelectronic and renewable energy applications, *J. Solid State Chem.* **301** (2021) 122294, https://doi.org/10.1016/j.jssc.2021.122294.

66. T. H. Flemban, V. Singaravelu, A. A. S. Devi and I. S. Roqan, Homogeneous vertical ZnO nanorod arrays with high conductivity on an in situ Gd nanolayer, *RSC advances* **5** (2015) 94670, https://doi.org/10.1039/C5RA19798H.

67. M. Sajjad, N. Singh, S. Sattar, S. De Wolf and U. Schwingenschlogl, Ultralow Lattice Thermal Conductivity and Thermoelectric Properties of Monolayer Tl2O, *ACS Applied Energy Materials* **2** (2019) 3004, https://doi.org/10.1021/acsaem.9b00249.